Aerobic oxidative coupling of amines to imines by mesoporous copper aluminum mixed metal oxides via generation of Reactive Oxygen Species (ROS)

Deepamali Dissanayake[a], Laura A. Achola[a], Peter Kerns[a], Dinithi Rathnayake[a], Junkai He[a], John Macharia[a], Steven L. Suib[a,b,*]

[a] Department of Chemistry, University of Connecticut, U-3060, 55 North Eagleville Road, Storrs, CT, 06269-3060, USA
[b] Institute of Materials Science, 97 North Eagleville Road, University of Connecticut, Storrs, CT, 06269-3136, USA

ABSTRACT

A mesoporous, monomodal copper aluminum mixed metal oxide (MMO) (average pore size 9.63 nm, surface area 140 m^2/g) synthesized via a modified inverse micelle method, efficiently catalyzes aerobic oxidative coupling of amines to imines. This material exhibits excellent conversion (> 99%) and selectivity (> 99%) towards imine synthesis under mild, solvent free, green conditions utilizing atmospheric air as the sole oxidant. Catalytic activity is observed for a diverse range of amine substrates. The aerobic oxidation of amines to imines follows a unique mechanistic pathway which involves Reactive Oxygen Species (ROS).

1. Introduction

Imines, otherwise known as Schiff bases, are important compounds in chemistry as well as in biology, because they are used as starting materials and intermediates for a number of organic transformation reactions, synthesis of bio-active nitrogen-containing compounds, and nitrogen heterocycles [1]. This class of compounds is widely recognized in a vast range of disciplines such as the pharmaceutical industry, agrochemical industry, and synthesis of fine chemicals, dyes, fragrances, and fungicides [2]. Over the past decade scientists have been trying to overcome disadvantages such as high energy consumption, waste by-products, and complications in operation and purification steps of the traditional method used in the synthesis of imines [3]. Therefore, attempts are taken in order to replace the traditional condensation reaction of carbonyl compounds and amines by introducing facile, direct, one pot methods such as aerobic oxidation of amines. Aerobic oxidation of amines is one of the most convenient alternative methods for imine synthesis and many catalytic systems have been reported as capable catalysts. Noble metal catalyst systems such as Pt, Au and Pd [4–6], Ru complexes [7], Cu catalysts [8–11], metal organic frameworks (MOF) [12], CeO$_2$ systems [2,13,14], MnO$_x$ catalysts [15], photocatalysts such as TiO$_2$ [16], graphene oxide (GO) [17,18], and mesoporous C [19] are among the already established catalytic systems. The majority of these catalysts are either expensive or toxic, have poor yields or selectivity, require co-catalysts, oxidants, high pressure, the presence of oxygen, or use solvents or other reagents which are harmful to the environment.

The conventional homogeneous mechanistic pathway for the synthesis of imines from primary amines consists of three major steps. Such paths usually involve initial oxidative addition of amines to the catalyst, followed by reductive elimination followed by either direct reaction with or hydrolysis into aldehydes, followed by condensation with the starting amine to produce imine products [3,20]. In addition, most of the heterogeneous systems and some homogeneous catalysts also report radical mediated mechanistic pathways involving ROS for this synthesis route [3,12,18,21–23]. But most of these radical mediated ROS involved mechanisms are observed in photocatalytic systems, electrochemical systems, MOFs, GO, Ionic liquids or when radical initiators are present [3]. Instances where ROS generation has been reported for thermally driven heterogeneous catalysis are fairly limited, even for other organic transformation reactions [10,11,23–25].

Mesoporous metal oxides are well known for their significant roles as heterogeneous catalysts for a vast number of organic reactions. Apart from the ability to be easily removed from a reaction mixture, their narrow pore sizes and shapes, high surface areas, and higher concentrations of active sites play important roles in making this class of catalysts industrially feasible. Mixed metal oxides are oxides containing two or more metal cations. They may exist as a single oxide having

multiple metal cations or as a mixture of two or more metal oxides, which is also known as a solid solution. These are well known for their versatile applications in ceramics, electronics, nuclear research, and especially in catalysis [26].

Among many reported mesoporous metal oxides, mesoporous mixed metal oxides are highly recognized as excellent catalysts for a number of organic reactions [1,26,27]. Sometimes for certain oxides the activity is substantially better when present in a mixed metal oxide than when acting as the sole catalyst for a reaction. This may be due to the fact that one can fine tune the number of acidic and basic sites present in the catalyst by introducing a new metal, allowing the oxide mixture to facilitate multiple steps of an organic transformation which favor acidic and basic environments during different steps of the reaction.

Many methods have been adopted for the synthesis of mixed metal oxides [26], namely, sol-gel methods [28,29], hydrothermal or solvothermal methods [30,31], wet impregnation [32,33], ion exchange [33], co-precipitation [34] [35], microwave irradiation [36], and mechanochemical synthesis [37,38]. On the other hand, soft templating sol-gel methods using amphiphilic molecules as the template are known as one of the most efficient approaches to synthesize mesoporous materials [39]. Among them, the inverse micelle method reported by Suib et al. [40] is known to be a promising method to obtain mesoporous materials with controllable pore sizes, surface area, and crystallinity. Although the method is widely utilized to obtain excellent mesoporous materials of a number of transition metals, such as mesoporous manganese oxides [41,42], cobalt oxide [43], titanium oxide [44,45] and iron oxides [46,47], instances where the method is used for the synthesis of mixed metal oxides are fairly infrequent [48]. The major challenge in adopting the method in mixed metal oxide synthesis is the insolubility of mixtures of metal precursors in the comparatively non-polar solvent system used.

As defined by the United States Environmental Protection Agency (EPA) green chemistry is the design of chemical products and processes that reduce or eliminate the use or generation of hazardous substances [49]. According to principles of green chemistry established by EPA, solvent free, reusable synthetic routes with minimum use of additives are highly desirable.

Herein, we report details about the synthesis of mesoporous, monomodal copper aluminum mixed metal oxide using a solvent modification with the inverse micelle method. This solvent modification allows the existing method to be used with metal precursors which are insoluble in the original method [40]. Details about how introducing minimal amounts of polar solvents can affect the mesoporosity and pore size are reported. Furthermore, application of this material as an inexpensive, reusable, and environmentally friendly, heterogeneous catalyst for imine synthesis by oxidative homocoupling and heterocoupling of primary amines under mild, solvent free, green conditions using atmospheric air as the sole oxidant is also discussed along with a study of the mechanism, which involves ROS. We elaborate how this thermally driven catalytic transformation of amine to imine is happening via generation of ROS - especially singlet oxygen, following a pathway which is often followed by photocatalysts [21,22]. This comparatively easy to produce catalytic system, evolves as a better system among other equally efficient catalysts, because it does not require any additives, a solvent, any additional oxidant other than atmospheric air, and its unique ROS involving mechanistic pathway with singlet oxygen in a thermal environment, which has not been reported so far.

2. Experimental section

2.1. Synthesis of mesoporous Cu /Al mixed metal oxide

In a typical synthesis, 0.01 mol of aluminum precursor (aluminum sec-butoxide (butox) or aluminum nitrate nonahydrate (nit)) was reacted with 0.134 mol of 1-butanol, 0.00034 mol of P123 (poly(ethylene glycol)-block-poly(propylene glycol)-block-poly(ethylene glycol),

Pluronic P123 or $PEO_{20}PPO_{70}PEO_{20}$ and 0.032 mol of conc. nitric acid. A solution of 0.01 mol of copper(II) nitrate trihydrate dissolved in 0.006 mol of solvent (methanol (meth), ethanol (eth) or 1-butanol (1-but)) was added into the mixture and well stirred at room temperature. The resulting blue-green solution was kept in an oven at 120 °C under air. After 3–4 h a blue-green solid product was collected, washed with ethanol several times and was kept in a vacuum oven at room temperature overnight. Finally, the resulting blue-green powder was subjected to two heating cycles, first at 150 °C for 12 h and then at 550 °C for 5 h under air. The final product was denoted as $Cu_{solvent\ dissolved}Al_{precursor}$.

2.2. Catalyst characterization

The physical, chemical, and morphological nature of the materials were investigated using a number of different characterization techniques. Powder X-ray diffraction (PXRD) measurements were performed on a Rigaku Ultima IV diffractometer (Cu Kα radiation, λ = 1.5406 Å, voltage of 40 kV and current of 44 mA). The PXRD patterns were collected over a 2θ range of 5–75 ° with a continuous scan rate of 2.0 °/min. The Nitrogen sorption experiments were performed using a Quantachrome Autosorb iQ$_2$ instrument using N_2 gas as the adsorbate at 77 K by a multipoint method. Prior to the analysis, all the samples were degassed at 150 °C for 5 h (ramp rate 10 °C/min) under helium in order to remove any adsorbed species. The surface area was calculated using the Brunauer − Emmett − Teller (BET) method, and the pore size and pore volume were calculated using the Barrett − Joyner−Halenda (BJH) method using the desorption branch of the isotherm.

The surface morphology was determined by SEM (Scanning Electron Microscopy), using an FEI Nova NanoSEM 450 with a Schottky emitter at an accelerating voltage of 2.0 kV having a beam current of 2.0 mA. EDX (Energy Dispersive X-ray Spectroscopy) was done using an Oxford AZtecEnergy Microanalysis system with X-Max 80 Silicon drift detector.

High-resolution transmission electron microscopy (HRTEM) experiments were carried out on a Talos F200X microscope at an operating voltage of 200 kV. The samples were prepared by casting the suspension of material onto a carbon-coated copper grid.

X-ray photoelectron spectra (XPS) characterization of the synthesized materials were done on a PHI model Quantum 2000 spectrometer with a scanning ESCA multiprobe (φ Physical Electronics Industries Inc.), using Al Kα radiation (λ = 1486.6 eV) as the radiation source. The spectra were recorded in the fixed analyzer transmission mode with pass energies of 187.85 eV and 29.35 eV for recording survey and high-resolution spectra, respectively. The powder samples were pressed on a double-sided carbon tape mounted on an Al coupon pinned to a sample stage with a washer and screw and then placed in the analysis chamber. Binding energies (BE) were measured for Cu 2p, Al 2p, Cu LMM (Auger), and O 1 s. The XPS spectra obtained were analyzed and fitted using CasaXPS software (version 2.3.16). Sample charging effects were eliminated by correcting the observed spectra with the C 1 s BE value of 284.8 eV.

For XRF (X-ray Fluorescence spectrometry), a Rigaku ZSX Primus IV sequential wavelength dispersive XRF spectrometer with a tube above geometry and an ultra-thin end window having an X-Ray tube with a 4 kW Rh anode was used. UV–vis spectra were obtained using the UV − Vis spectrophotometer, Shimadzu UV − Vis 2450. Photoluminescence spectra were obtained using a FluoMax Plus spectrofluorometer by Horiba Scientific.

2.3. Catalytic activity measurements

2.3.1. Oxidative homocoupling of amines

A mixture of amine (3 mmol) and catalyst (100 mg) was added into a 25 mL round-bottom flask equipped with a condenser. The reaction mixture was heated in an oil bath to reflux under vigorous stirring under air atmosphere for the required time. The round bottom flask was

cooled after the completion of the reaction and the product was collected by filtration. The product was analyzed using GC/MS (gas chromatography/mass spectrometry). The GC/MS analysis was performed with a 7820 A GC system connected to a mass detector of 5975 series from Agilent Technologies and a nonpolar cross-linked methyl siloxane column with dimensions of 12 in × 0.200 mm × 0.33 μm. The conversion was determined with respect to the percent amount of the amine. Selectivity was determined with respect to any other products present, if any. TON and TOF were calculated after the completion of reaction. For confirmation of products ^{1}H and ^{13}C NMR (Nuclear Magnetic Resonance spectroscopy) were obtained and these spectra were recorded on a Bruker AVANCE III- 400 MHz spectrometer and 300 MHz spectrometer respectively. ^{1}H NMR spectra were collected at 400 MHz with chemical shifts referenced to the residual peak in $CDCl_3$ (δ: H 7.26 ppm). ^{13}C NMR spectra were collected at 300 MHz and referenced to the residual peak in $CDCl_3$ (δ: C 77.0 ppm).

2.3.2. Oxidative heterocoupling of amines

In a typical synthesis, 3 mmol of benzylamine, 3 mmol of the other amine, and the catalyst (100 mg) were added into a 25 mL round bottom flask equipped with a condenser. The reaction mixture was heated in an oil bath to reflux under vigorous stirring under air atmosphere for the required time. The round bottom flask was cooled after the completion of the reaction and the product was collected by filtration. The product was then analyzed using GC/MS.

2.3.3. ROS (Reactive Oxygen Species) and other radical activity studies

The presence of hydroxy radical, ˙OH, was investigated by reacting 0.4 mmol of the reaction mixture with 0.005 mmol of disodium terephthalate (DST), 0.05 mmol of NaOH, and incubating for 50 min. followed by photoluminescence studies. The presence of singlet oxygen, $^{1}O_2$, was investigated by collecting the reaction mixture after 1 h and treating with 0.4 mmol of Singlet Oxygen Sensor Green (SOSG) followed by photoluminescence studies. The presence of superoxide anion, O_2˙$^{-}$, was investigated by collecting the reaction mixture after 1 h and treating with 0.04 mol of nitro blue tetrazolium chloride (NBT) followed by UV–vis studies. Finally, the presence of H_2O_2 was investigated by collecting the reaction mixture after 1 h and treating with $1.3 * 10^{-6}$ mol of leucocrystal violet (LCV) in the presence of horseradish peroxidase (HRP) in a buffered system (acetate buffer at pH 4.5) followed by UV–vis studies.

3. Results

The PXRD spectrum for $Cu_{meth}Al_{butox}$ (Fig. 1) and other Cu Al samples (Fig. S. 1 in supporting information) showed similar peak

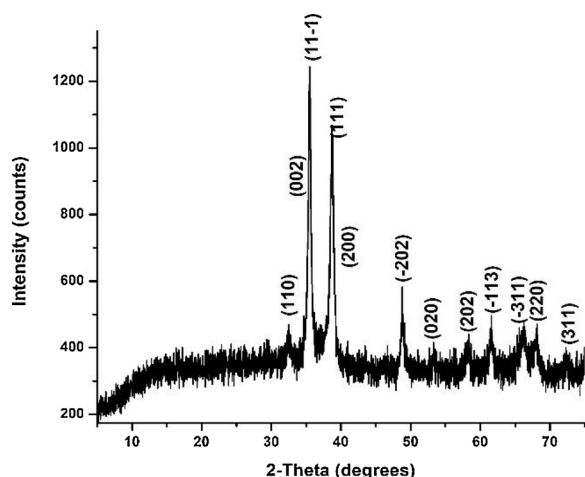**Fig. 1.** PXRD pattern for $Cu_{meth}Al_{butox}$.

patterns. The peak pattern was best assigned to that of CuO tenorite phase (PDF card no. 01-073-6023). Since no peaks for Al_2O_3 or any aluminum containing species were observed, different diffraction patterns were obtained by heating the sample up to a maximum of 1100 ˙C, holding the materials for 1 h at each given temperature. Peaks arising from the presence of aluminum were only observed upon increasing temperature above 650 ˙C (Fig. S. 2). Two different CuAl mixed metal oxides were observed from 750 ˙C - 850 ˙C and at 1100 ˙C, arising from $CuAl_2O_4$ spinel (pdf card no 00-033-0448) and $CuAlO_2$ delafossite (pdf card no 01-075-2356) respectively. To check the mesoporosity of the synthesized materials N_2 sorption studies were done. $Cu_{meth}Al_{butox}$ showed a type IV adsorption isotherm with a H1 type hysteresis loop (Fig. 2 a) while all other CuAl samples gave type IV adsorption isotherms with H3 type hysteresis loops (Fig. S. 3). Pore size distribution (BJH method) of $Cu_{meth}Al_{butox}$ showed a pore size of 9.53 nm and was monomodal in nature (Fig. 2 b). None of the other Cu Al MMO (Mixed Metal Oxides) samples showed monomodal character and some were macroporous in nature (Fig. S. 4). The best surface area was also observed for the same material, which was 140 m^2/g (Table 1). Therefore, the pore size, pore volume, and surface area of the materials varied greatly with solvent and precursor (Table 1). All other characterization techniques were carried out for the best mesoporous Cu Al sample which was $Cu_{meth}Al_{butox}$.

SEM images of $Cu_{meth}Al_{butox}$ consisted of two morphologies (Fig. 3 a) and further magnification of the two morphologies showed random aggregates of bead-like structures (Fig. 3 b) and asymmetrical blocks with rough surfaces (Fig. 3 c). TEM imaging (Fig. 4) showed random packing of the mixed metal oxide material without any long-range order.

The survey XPS spectrum of $Cu_{meth}Al_{butox}$ (Fig. 5) showed peaks for Cu, Al, and O species. Cu 2p spectra (Fig. S. 5 a) consisted of four peaks and two satellite peaks. Cu $2p_{3/2}$ peaks were observed at 931.6 eV, 933.2 eV, and Cu $2p_{1/2}$ peaks were at 951.8 eV and 953.7 eV respectively. Additionally, the Cu LMM spectrum showed a distinct peak at 917.6 eV as well (Fig. S. 5 b). For Al 2p, two peaks were observed at 164.3 eV and 196.7 eV respectively (Fig. S. 5 c). In addition, three peaks were observed for O 1 s at 529.3 eV, 531.4 eV, and 530.3 eV (Fig. 5 d). Furthermore, XRF data showed the presence of CuO (59.6% by mass) and Al_2O_3 (40.4%) (Table S. 2).

For the catalytic reaction, the CuAl MMO with the best mesoporosity and surface area, $Cu_{meth}Al_{butox}$ was chosen. All other materials in Table 1 were less active than $Cu_{meth}Al_{butox}$ (Table S. 1 entries 9–12). Therefore, for initial screening of catalytic activity, oxidative homocoupling of benzylamine was studied with the $Cu_{meth}Al_{butox}$ catalyst. Reaction conditions were optimized by changing the solvent, the amount of catalyst, time of reaction, and reaction temperature to obtain the highest selectivity and conversion. In addition, the reaction atmosphere was changed by using a balloon of air, O_2, and N_2 after vacuuming any residual air from the system. Details of the catalytic optimization study can be found in Table 2.

Among the solvents tested, acetonitrile and solvent free conditions showed the best activity and more environmentally benign solvent free conditions were chosen for the rest of the reactions (Table 2 entries 1–5). The best activity of the reaction was observed with 100 mg of catalyst and any further catalyst loading did not increase the percent conversion (Table 2 entries 6,7). The percent conversion of the reaction did not improve upon increasing the reaction time above 15 h but dropped to 75% upon decreasing to 12 h (Table S. 1 entries 1–3). Dropping the temperature below 100 ˙C (90 ˙C) reduced the percent conversion to 77% and increasing the temperature above 110 ˙C did not result in a better conversion (Table S. 1 entries 4–6).

When the reaction was carried out with commercial CuO or commercial Al_2O_3 as the sole catalyst very low conversions were observed (Table S. 1 entries 7,8). The effect of oxidant and amount of oxidant were tested by attaching a balloon of O_2, N_2, or air to the condenser (Table 2 entries 9–11). O_2 and air balloons had similar effects as
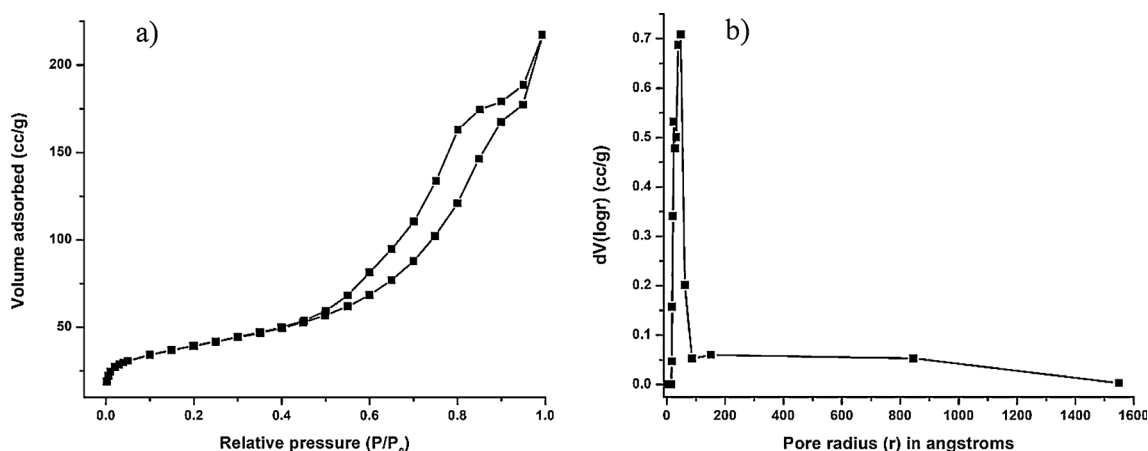
Fig. 2. a) BET isotherm of $Cu_{meth}Al_{butox}$ b) BJH pore size distribution of $Cu_{meth}Al_{butox}$.

Table 1
Solvent and precursor effects on the surface area, pore volume, and pore diameter.

Catalyst	BET surface area (m^2/g)	BJH pore volume (cm^3/g)	BJH pore diameter (nm)
$Cu_{meth}Al_{nit}$	48	0.203	16.7
$Cu_{eth}Al_{nit}$	28	0.163	23.1
$Cu_{1-but}Al_{butox}$	13	0.098	28.5
$Cu_{eth}Al_{butox}$	130	0.650	9.53
$Cu_{meth}Al_{butox}$	140	0.344	9.63

Fig. 4. TEM image of $Cu_{meth}Al_{butox}$.

refluxing with atmospheric air while the presence of inert N_2 gas drastically dropped the catalytic activity. In order to find out if this particular material has an effect on the desired reaction, a 1:1 M mixture of commercial CuO and Al_2O_3 was used in the reaction under similar conditions. The commercial mixture showed a very low conversion compared to our catalyst.

After the reaction conditions were fully optimized, substrate scope was explored in order to find out how different substituents, aliphatic and aromatic systems, sterically hindered reactants and less bulky reactants can be catalyzed (Table 3). The scope of catalysis, when one or more electron donating groups such as $-CH_3$, $-OCH_3$ are attached to the benzene ring was studied along with electron withdrawing substituents such as $-F$, $-Cl$ and $-CF_3$.

In addition, the effects of ortho, para, and meta substituents were explored using $-OCH_3$ groups substituted at different positions of the benzylamine ring. The electron donating groups (Table 3 entries 1–4) had lower activities, which displayed relatively lower TOFs (Turn Over Frequency) towards the reaction compared to unsubstituted benzylamine. Meanwhile, when electron withdrawing groups were used as
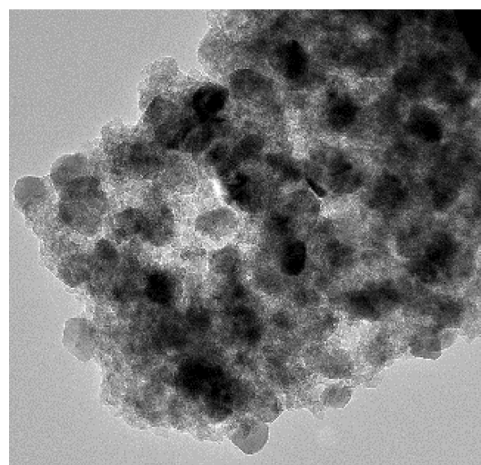
substituents, better catalytic properties were observed, hence, better TOFs compared to that of benzylamine were displayed (Table 3 entries 5–8). When sterically hindered α-methylbenzylamine and 1-naphthylmethylamine substrates were examined, less TOFs or no reactivity was observed (Table 3 entries 9,14) respectively. The catalyst was efficient but less active towards aromatic heterocyclic compound, 2-thiophenemethylamine compared to benzylamine (Table 3 entry 11). The catalyst was equally active towards secondary amines including cyclic amines as well (Table 3 entries 10,12). But the catalyst was totally inactive towards aliphatic amines (Table 3 entries 13). The presence of these products was also confirmed by ^{1}H NMR and ^{13}C NMR (supporting information).
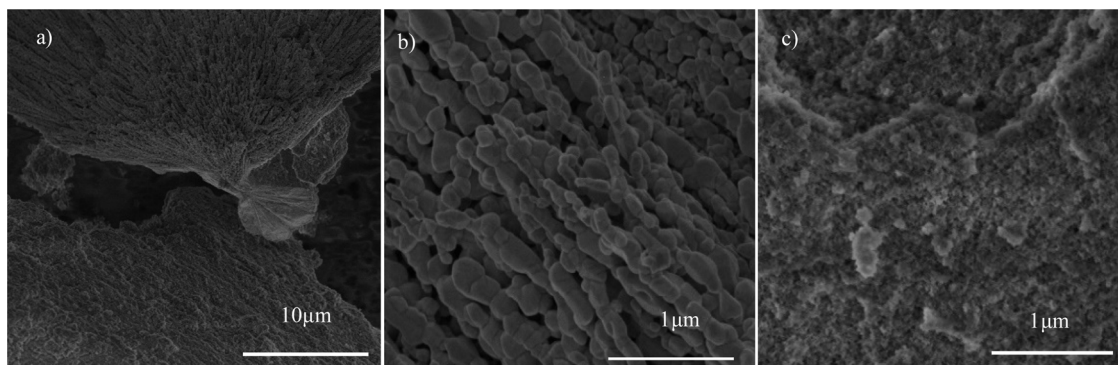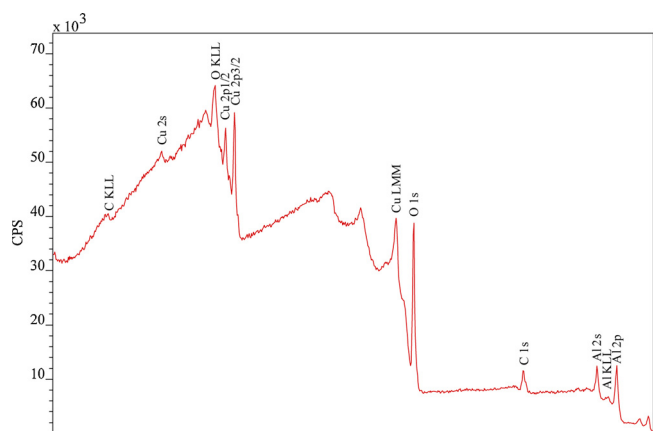

Fig. 3. SEM images of $Cu_{meth}Al_{butox}$.

Fig. 5. XPS full range spectrum of $Cu_{meth}Al_{butox}$.

After observing the activity of the catalyst towards a vast scope of substituents, the applicability of the catalyst in oxidative hetero-coupling was also explored (Table 4). When two different primary benzylamines are reacted, four products are possible, out of which, two are homocoupled products (**b** and **d**) of the two amines reacted, and the other two are heterocoupled products of one amine with the other (**a** and **c**). For a number of different substituents, our catalyst showed excellent conversion when two different amines are reacted but, the selectivity towards the desired heterocoupled product showed average values ranging from 17%–52% (Table 4). Further, it was hard to observe any particular trend with the nature of the substituent.

Since reusability and negligible to no leaching are two of most important aspects of heterogeneous catalysts, reusability, and leaching tests were performed for the oxidation of benzylamine by following standard methods (Graph S. 1, Graph S. 2). The activity of the catalyst was well preserved even after the 5th cycle. In addition, no changes were observed in the PXRD patterns obtained before and after the reaction (Fig. S. 7). No leaching was observed in the catalytic system (Graph S. 1).

Experiments were also carried out in order to investigate the mechanism and kinetics of the reaction. Several ROS and a radical cationic intermediate were observed using well known detection methods reported in the literature [50]. When treated with nitro tetrazolium blue chloride (NBT), a characteristic UV–vis peak in between 450–700 nm for superoxide anion was observed (Fig. S. 10 a). Hydroxyl radical was

observed by the characteristic fluorescent peak at 400–500 nm in the presence of disodium terephthalate (DST) (Fig. S. 10 c). In the presence of leucocrystal violet (LCV), a characteristic UV–vis peak at 596 nm was observed (Fig. S. 10 b), revealing the presence of H_2O_2 in the system, while the presence of singlet oxygen was observed by the characteristic fluorescence peak at 550 nm using singlet oxygen sensor green (SOSG) (Fig. S. 10 d). Time and temperature dependent studies revealed that the reaction follows first order kinetics with a rate constant of 0.053 h^{-1}. The activation energy of the reaction was calculated to be 11.72 kJ mol^{-1} by Arrhenius plot calculations.

4. Discussion

4.1. Catalyst characterization

Our modified inverse micelle sol-gel method involves loading of metal ion precursors into inverse micelles, which upon heat treatment would give rise to mesoporous structures. Initially, bimetallic ion clusters are stabilized inside the hydrated inverse micelles formed by the surfactant P123 via hydrogen bonding. These inverse micelles act as nanoreactors for the formation of the final mesoporous material. The hydrotropic NO_3^- ion is responsible for hydrating the inverse micelles, drawing the oppositely charged metal cation clusters into the micelle. The original method uses the non-polar solvent 1-butanol as the interface modifier which is responsible for lessening the number of aggregates [40]. In this study, a very small amount of methanol or ethanol solvents has been introduced in order to increase the polarity of the solvent system and to increase the solubility of the metal precursors without sacrificing the mesoporosity of the material. Interestingly, introduction of ethanol destroys the mesoporosity, while methanol acts as a good candidate for the desired task. Since the nature of polarity of these two solvents is almost similar to each other, the smaller size of methanol gives a better penetrating ability into the micelle which then acts as an additional interface modifier and solvent alongside 1-butanol. These inverse micelles would form NO_x upon heat treatment at 120 °C, due to the thermal decomposition of NO_3^-, which would increase the pH of the system. Then the solvent extraction by ethanol would remove the surfactant from the material and finally, the calcination steps remove chemisorbed species giving rise to a mesoporous material [15].

The original inverse micelle sol gel method can be successfully modified by the secondary solvent methanol to expand the applicability towards relatively insoluble, challenging metal precursors. Further studies are being carried out in order to understand how this
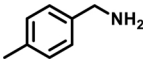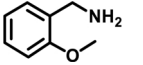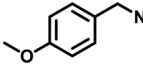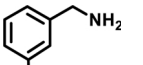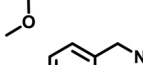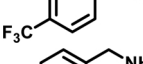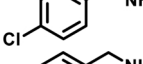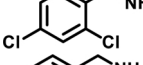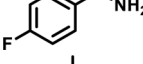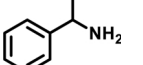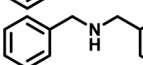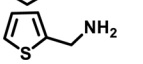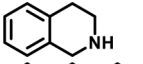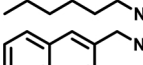
Table 2
Catalytic optimization study of benzylamine by $Cu_{meth}Al_{butox}$.

Entry	Solvent	Temp (°C)	Time (h)	Cat.amount (mg)	Conversion (%)	Selectivity (%)	TON	TOF
1	Toluene	110	20	50	86	21	1.96	0.01
2	Acetonitrile	80	20	50	67	> 99	7.28	0.36
3	Ethanol	80	20	50	22	80	1.91	0.01
4	Hexane	70	20	50	2	> 99	0.22	0.01
5		100	20	50	70	> 99	7.60	0.38
6		100	20	75	82	> 99	5.94	0.30
7		100	20	100	> 99	> 99	5.43	0.27
8		100	15	100	> 99	> 99	5.43	0.36
9[b]		100	15	100	> 99	> 99	5.43	0.36
10[c]		100	15	100	> 99	> 99	5.43	0.32
11[d]		100	15	100	23	> 99	1.24	0.08
12[e]		100	15	N/A	10	30	N/A	N/A
13[f]		100	15	100	28	> 99	1.52	0.15

Reaction conditions: benzylamine (3 mmol), $Cu_{meth}Al_{butox}$, solvent (3 mL), refluxed under atmospheric air. [b] air balloon, [c] O_2 balloon, [d] N_2 balloon, [e] no catalyst, [f] 1:1 mixture of commercial CuO and Al_2O_3. other by products were aldehyde, carboxylic acid and cyanide. TON = moles of amine converted per mole of catalyst. TOF = TON per one hour of reaction.

Table 3
Catalytic oxidative homocoupling of different amine substrates over $Cu_{meth}Al_{butox}$.

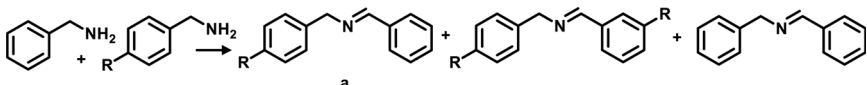| Entry	Substrate	Time (h)	Selectivity (%)	Conversion (%)	TON	TOF
1	(structure)	16	> 99	> 99	5.43	0.34
2	(structure)	16	> 99	> 99	5.43	0.34
3	(structure)	16	> 99	> 99	5.43	0.34
4	(structure)	15	> 99	> 99	5.43	0.36
5	(structure)	13	> 99	> 99	5.43	0.42
6	(structure)	13	> 99	> 99	5.43	0.42
7	(structure)	12	> 99	> 99	5.43	0.45
8	(structure)	12	> 99	> 99	5.43	0.45
9	(structure)	15	> 99	68	3.69	0.25
10	(structure)	15	> 99	> 99	5.43	0.36
11	(structure)	16	> 99	> 99	5.43	0.34
12	(structure)	15	> 99	> 99	5.43	0.36
13	(structure)	20	nd	nd	nd	nd
14	(structure)	20	nd	nd	nd	nd

Reaction conditions: amine substrate (3 mmol), $Cu_{meth}Al_{butox}$ (100 mg), refluxed under atmospheric air. Other by-product was uncoupled intermediate imine. TON = moles of amine converted per mole of catalyst. TOF = TON per one hour of reaction. nd = not detected.

Table 4
Catalytic oxidative heterocoupling of different amine substrates with benzylamine over $Cu_{meth}Al_{butox}$.

(reaction scheme)

Entry	Substrate (R)	Time (h)	Conversion	Selectivity of **a/c** (%)	TON	TOF
1	-CH₃	16	> 99	44	2.39	0.15
2	ortho-OCH₃	16	> 99	21	1.14	0.07
3	para-OCH₃	16	> 99	52	2.82	0.17
4	meta-OCH₃	16	> 99	22	1.19	0.01
5	-F	15	> 99	37	2.00	0.13
6	-CF₃	15	> 99	36	1.95	0.13
7	-Cl	15	> 99	35	1.90	0.13
8	2,4-dichloro benzylamine	15	> 99	39	2.12	0.14
9	hexylamine	15	> 99	17	0.92	0.06

Reaction conditions: amine substrate (3 mmol) and benzylamine (3 mmol), $Cu_{meth}Al_{butox}$ (100 mg), refluxed under atmospheric air. TON = moles of amine converted per mole of catalyst. TOF = TON per one hour of reaction.

modification can be generalized further.

For the samples calcined at 550 °C, PXRD data only showed peaks for the CuO tenorite phase [1,51]. Interestingly, no alumina peaks were observed until the material was heated to 750 °C. At 550 °C, Al_2O_3 is not crystalline enough and appears to be amorphous in nature, thus, would not give rise to any PXRD peaks. Our observation agrees well with the literature, [52] where sintering a mixture of CuO/Al_2O_3 powders has been used as a method to synthesize the pure phases of cuprous aluminate ($CuAlO_2$) and copper alumina spinel ($CuAl_2O_4$). N_2 sorption studies were used as a measure of mesoporosity of the materials synthesized. All except $Cu_{meth}Al_{butox}$ exhibit type IV isotherms with H3 hysteresis loops, which are representative of the presence of

aggregates of particles forming slit-shaped pores [53].

None of these materials showed a monomodal nature and almost all showed some macropores as well. This confirms that these precursor - solvent combinations are unable to preserve the original characteristics of the inverse micelle method. Whereas the sample prepared with methanol as the solvent and aluminum sec-butoxide as the aluminum precursor, $Cu_{meth}Al_{butox}$, showed a type IV isotherm with an H1 hysteresis loop, showing excellent mesoporosity with an average monomodal pore diameter with 9.63 nm and a high surface area of 140 m^2/g. The best material $Cu_{meth}Al_{butox}$ was further characterized and SEM and TEM imaging showed that two morphologies are present without any long-range order.

This observation of two morphologies further confirms that two metal oxides are present instead of one although the sample is too amorphous to show peaks arising from Al in the PXRD pattern. Furthermore, EDX elemental mapping (Fig. S. 6) showed a random dispersion of Cu and Al. Certain areas of the material showed higher amounts of Cu while some showed higher percentages of Al, further confirming the presence of the mixture of two metal oxides, CuO and Al_2O_3. The Cu 2p XPS spectrum showed a pattern with two satellite peaks which are characteristic of CuO. Auger Cu LMM spectra further confirmed this by showing the identical Cu^{2+} CuO peak at 917 eV [53]. In addition, Al 2p peaks observed at 73.5 eV and 75.9 eV can be assigned to Al_2O_3 [54]. The O1 s spectrum showed three peaks at 529.3, 531.4, 530.3 eV which can be assigned to CuO, Al_2O_3, and Al_2O_3 respectively, confirming the existence of the presence of the two metal oxides in solid solution. XRF data were obtained to further confirm the presence of CuO and Al_2O_3 and roughly, a 1:1 M ratio was observed.

4.2. Catalysis of amine oxidation

Synthesized CuO/Al_2O_3 catalysts were successfully utilized in catalytic aerobic oxidation of amines to imines. The best catalytic activity was observed for the catalyst with best surface area and mesoporosity, $Cu_{meth}Al_{butox}$, showing that these two properties are crucial factors governing the catalytic activities of these catalysts. High surface area of the catalyst $Cu_{meth}Al_{butox}$ with a higher number of available catalytic sites for the reaction to occur shows the highest conversion. A vast collection of amines was efficiently converted into imines over this catalyst. This collection includes challenging substrates such as halobenzene derivatives (Table 3 entries 5–8) which usually dehalogenate [55] before other reactions occur; amines with heteroatoms (S) (Table 3 entry 11) - known for catalyst poisoning by strong coordination of the heteroatom to the transition metal [56]; ortho, para, and meta substituted benzylamines (Table 3 entries 2–4); electron donating and withdrawing substituents; and even comparatively inert secondary amines.

Blank runs containing no catalyst showed very little conversion (10%) (Table 2 entry 12), showing that the catalyst is crucial for the reaction to occur. Under inert N_2, 23% conversion was observed showing the participation of lattice oxygen in the oxidation (Table 2 entry 11) as reported with many mesoporous oxide catalysts [15,23,24,57]. Similar results were also observed when the reaction was facilitated with an external source of O_2, air, or having atmospheric air in the condenser. These results confirm that the presence of catalyst and atmospheric air can result in the completion of the reaction without the need for any co-catalyst or additional oxidant. These simple reaction conditions together with comparatively lower temperature, and most importantly the absence of the use of any solvent makes this system an environmentally friendly, green system for the synthesis of an important class of organic compounds which is more desirable than most of the already reported, equally efficient, less environmentally benign catalytic systems which require the presence of solvents [10,11,15,58], additional oxidants or co-catalysts [19,59] or complicated material synthesis procedures [18].

When electron donating, activating groups were substituted in the

para position of the benzylamine, higher TOFs were obtained. When deactivating, electron withdrawing groups were present, the percent conversion was intact, but lower TOFs were obtained. This result was consistent with some reported catalytic systems, where the formation of a negatively charged species occurs at an intermediate step which has the most impact on the rate of the reaction [3,15]. When ortho, para, and meta substituents were considered, ortho and para substituents have a similar effect on the reaction rates, showing similar TOFs and the effects of meta substituents were relatively small. This shows that ortho and para substituents can have an effect on the suspected negatively charged species while meta substituents are having little or no effect.

The relatively challenging secondary amines (Table 3 entries 10, 12) were converted to their respective imines with a very high efficiency as long as the imine formation is intermolecular. However, the imine formation of α-methylbenzylamine (Table 3 entry 9) was not selective, due to the steric effect of the bulkier benzyl and methyl substituents. The approach of the second molecule for coupling must be strongly hindered by steric effects. This is even further confirmed by the reaction of 1-methylnaphthylbenzylamine (Table 3 entry 14), which was a much bulkier primary amine which showed no reaction towards aerobic oxidation. Aliphatic amines (Table 3 entry 13) showed no activity towards the reaction due to their inactive nature towards the reaction which is observed in many catalytic systems reported [15].

Synthesis of asymmetric imines showed excellent percent conversions for a vast variety of different substituents, including inert aliphatic amines. But the reactions suffered from lower percent selectivities toward the desired heterocoupled products (Table 4 product **a** or **c**). Selectivities of these hetero-coupled products depend on the likelihood of the two competing amines to oxidize in to the intermediate imine and coupling of this intermediate imine with one of the starting amines. This ability of oxidation of the amine can depend on various factors including steric factors or the bond dissociation energy of the C–H bond adjacent to the N atom [62] or the ability of the catalyst to selectively oxidize one amine over the other. In this case, poor correlation between the selectivity values between different substituents suggests that the catalyst is not extremely selective towards one substrate when more than one amine is present. However, since the conversion was exceptionally good, with proper adaptation of separating techniques, this catalyst could be a useful tool for cross-coupling reactions as well. A mechanism can be suggested for the reaction depending on the literature and the observations for this particular catalytic system.

Depending on the ROS investigation, and substrate scope study, a plausible mechanism can be proposed for the homocoupling reaction of amines (Scheme 1). Observing the effects exerted on the TOF by different electron withdrawing and electron donating substrates, commonly reported [12,15,21–24,57,18,60–62] radical cationic intermediated species **1b**, which leads to the negatively charged species **1c** was anticipated. In order to confirm the presence of this radical intermediate, a well known [23–25] radical trapping agent BHT (2,6-di-tert-butyl-4- methylphenol) was used and the adduct of the trap and radical cationic species **1b** was observed in the mass spectrum in good yield (Fig. S. 8). The formation of this cationic radical intermediate is likely driven by the presence of CuO, where the Cu^{2+} is converted to Cu^{+1} by removing an electron from the lone pair of nitrogen [24,25].

The catalyst is expected to regain its original Cu^{2+} oxidation state by producing an electron which is used in the formation of superoxide anion, $O_2^{.-}$ from O_2 in the air. This is supported by the differences seen in Cu 2p XPS spectra taken for the post-catalyst in an air environment and inert N_2 environment (Fig. S. 9 top) and the Auger Cu LMM spectra taken before and after the reaction (Fig. S. 5 and Fig. S. 9 bottom). The presence of Cu^{1+} is clearly visible in the N_2 environment post catalyst, with a much-broadened peak, due to the presence of two peaks arising from Cu^{1+} and Cu^{2+}. Additional peaks at 935.43 eV and 955.48 eV are attributed to Cu^{1+} from Cu_2O [53], whereas in a usual air environment a narrow peak is observed due to the presence of Cu^{2+} from CuO which
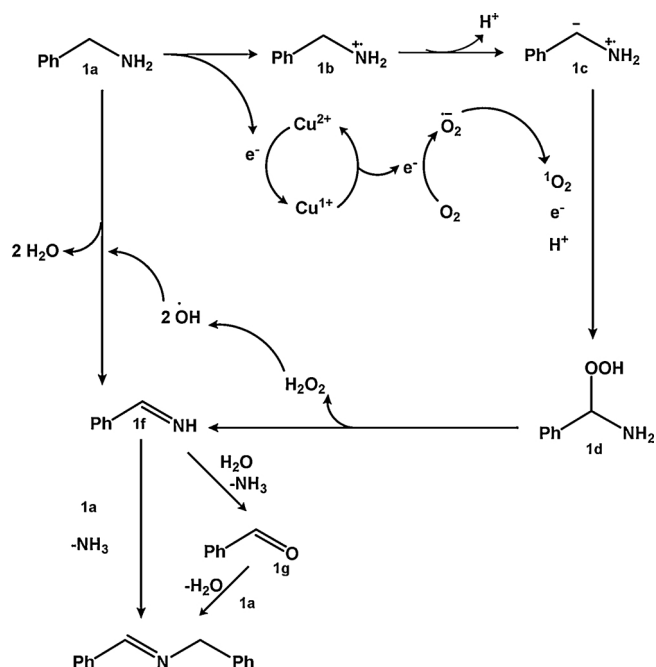
Scheme 1. Proposed mechanism for aerobic oxidative homocoupling of primary amines over the catalyst.

aligns well with the peaks for the catalyst before the reaction (Fig. S. 5 a). Similarly, Auger Cu LMM data showed similar binding energies around 917 eV, confirming that the original Cu^{2+} oxidation state of CuO is reinstated after the reaction [53]. Nevertheless, when the reaction environment is changed to inert N_2, the Cu LMM binding energy is shifted to 916 eV (Fig. S. 9 bottom), which is characteristic of the Cu^{+1} oxidation state of Cu_2O [53].

This further confirms our initial observation of 23% conversion when the reaction is carried out in an inert N_2 environment (Table S. 1 entry 11), which shows that lattice oxygen must be utilized in the reaction in the absence of O_2 in the air. In addition, when the O_2 supply is limited, the initial Cu^{2+} oxidation state is not easily reinstated, thus some of the initially converted Cu^{+1} can still be present in the catalyst. This led us to presume the catalytic cycle of CuO, which involves the conversion of molecular O_2 to $O_2^{\cdot-}$.

The presence of superoxide anion was confirmed by the characteristic UV–vis peak in between 450 − 700 nm [63] in the presence of nitro tetrazolium blue chloride (NBT) additive (Fig. S. 10 a). Singlet oxygen can be generated by losing an electron from superoxide anion [50,64–66]. Although this happens more often in light-mediated catalysis [64] and electrochemical catalysts [66], similar observations for thermally energized catalysis have not been reported so far. Previously reported similar thermally driven studies by our group often proceed via superoxide anion [23–25]. Interestingly, we observed the presence of singlet oxygen in the absence of light in the system, by the presence of a characteristic fluorescence peak at 550 nm using singlet oxygen sensor green (SOSG) (Fig. S. 10 d) showing the possibility of generating singlet oxygen from superoxide anion even in catalytic systems which utilize thermal energy. Cationic radical **1b** subsequently loses an α C–H proton in order to generate highly unstable species **1c**, which has been reported in previous studies [15,23,24] and explains the effects of electron donating and withdrawing groups. This highly unstable species then reacts with highly reactive singlet oxygen, producing **1d** [21], which forms a C=N bond by eliminating H_2O_2 which was detected by its characteristic UV–vis peak at 596 nm with leucocrystal violet (LCV) (Fig. S. 10 c).

By observing hydroxyl radical by the characteristic fluorescence peak around 440 nm in the presence of disodium terephthalate (DST)

(Fig. S. 10 b), we came to the understanding that H_2O_2 should be transformed into water via generation of hydroxyl radicals. On the other hand, this also gives rise to the possibility of a second pathway of forming **1f** directly from the starting material **1a**. The intermediate product **1f** generated, either way, must couple with another molecule of **1a**, either directly or after oxidizing into the aldehyde (**1 g**) in order to generate the desired final imine product.

Although alumina is not utilized in the proposed mechanism directly, the presence of acidic sites is beneficial for the final condensation step [67]. As alumina is a good support material, better results in the leaching study for this system could be due to the presence of alumina. Therefore, given its property as a good support material, its ability to incorporate an appropriate amount of acidity to the system, and 23% activity observed when commercial alumina is used as the sole catalyst (Table S. 1 entry 8), we are convinced that alumina further improves the activity of the system [12,58]. We are hoping to conduct further studies in order to investigate the contribution of acidic sites of alumina for the final condensation steps of the mechanism.

We also investigated the time and temperature dependent experiments on the catalytic oxidative homocoupling of benzylamine in order to study the reaction kinetics (Fig. S. 11). Samples were continuously collected per one hour in the course of 10 h at three different temperatures and conversion and selectivity were determined by GC/MS. Kinetic studies depicted a first-order rate equation with respect to the amine (Fig. S. 12) having a rate constant of 0.053 h^{-1}. Calculations done using Arrhenius plots (Fig. S. 13) showed that the activation energy for the reaction is 11.72 kJ mol^{-1}.

5. Conclusion

In summary, we have reported the synthesis and characterization of mesoporous copper aluminum mixed metal oxides using a modified inverse micelle method. Synthesized mixed metal oxide material is successfully utilized in the synthesis of imines by aerobic oxidative homocoupling of primary amines, as a highly efficient, selective, reusable, green and environmentally benign catalyst. The surface area of the material was as high as 140 m^2/g with a uniform monomodal mesoporous pore diameter distribution of 9.63 nm. The catalyst exhibited excellent conversion percentages (as high as > 99%) and selectivities (as high as > 99%) towards a versatile range of primary amines under mild solvent free conditions using atmospheric air as the sole oxidant. The material also showed the ability to catalyze oxidative hetero-coupling of primary amines by coupling benzylamine and other primary amine substrates with conversions as high as > 99% and good selectivities (ranging from 17%–52%). Our mechanistic investigation revealed the involvement of ROS in catalytic activity, produced from atmospheric O_2 by the active catalyst CuO.

Associated content

The Supporting Information. List of chemicals, additional PXRD, BET, EDS, XPS, XRF, kinetic study, reusability study, Leaching study, calculation of activation energy, and ^{1}H NMR and ^{13}C NMR of products.

Available free of charge (PDF)

Acknowledgments

(CAMMA).

Appendix A. Supplementary data

Supplementary material related to this article can be found, in the online version, at doi:https://doi.org/10.1016/j.apcatb.2019.02.037.

References

[1] M.N. Pahalagedara, L.R. Pahalagedara, D. Kriz, S.Y. Chen, F. Beaulieu, W. Thalgaspitiya, S.L. Suib, Copper aluminum mixed oxide (CuAl MO) catalyst: a green approach for the one-pot synthesis of imines under solvent-free conditions, Appl. Catal. B Environ. 188 (2016) 227–234, https://doi.org/10.1016/j.apcatb.2016.02.007.

[2] P. Sudarsanam, B. Hillary, M.H. Amin, S.B.A. Hamid, S.K. Bhargava, Structure-activity relationships of nanoscale MnO_x/CeO_2 heterostructured catalysts for selective oxidation of amines under eco-friendly conditions, Appl. Catal. B Environ. 185 (2016) 213–224, https://doi.org/10.1016/j.apcatb.2015.12.026.

[3] B. Chen, L. Wang, S. Gao, Recent advances in aerobic oxidation of alcohols and amines to imines, ACS Catal. 5 (2015) 5851–5876, https://doi.org/10.1021/acscatal.5b01479.

[4] J.R. Wang, Y. Fu, B.B. Zhang, X. Cui, L. Liu, Q.X. Guo, Palladium-catalyzed aerobic oxidation of amines, Tetrahedron Lett. 47 (2006) 8293–8297, https://doi.org/10.1016/j.tetlet.2006.09.088.

[5] B. Zhu, M. Lazar, B.G. Trewyn, R.J. Angelici, Aerobic oxidation of amines to imines catalyzed by bulk gold powder and by alumina-supported gold, J. Catal. 260 (2008) 1–6, https://doi.org/10.1016/j.jcat.2008.08.012.

[6] A. Grirrane, A. Corma, H. Garcia, Highly active and selective gold catalysts for the aerobic oxidative condensation of benzylamines to imines and one-pot, two-step synthesis of secondary benzylamines, J. Catal. 264 (2009) 138–144, https://doi.org/10.1016/j.jcat.2009.03.015.

[7] A. Taketoshi, T.A. Koizumi, T. Kanbara, Aerobic oxidative dehydrogenation of benzylamines catalyzed by a cyclometalated ruthenium complex, Tetrahedron Lett. 51 (2010) 6457–6459, https://doi.org/10.1016/j.tetlet.2010.10.004.

[8] J. Kim, S.S. Stahl, Cu/nitroxyl-catalyzed aerobic oxidation of primary amines into nitriles at room temperature, ACS Catal. 3 (2013) 1652–1656, https://doi.org/10.1021/cs400360e.

[9] B. Xu, E.M. Hartigan, G. Feula, Z. Huang, J.P. Lumb, B.A. Arndtsen, Simple copper catalysts for the aerobic oxidation of amines: selectivity control by the counterion, Angew. Chemie - Int. Ed. 55 (2016) 15802–15806, https://doi.org/10.1002/anie.201609255.

[10] L. Al-Hmoud, C.W. Jones, Reaction pathways over copper and cerium oxide catalysts for direct synthesis of imines from amines under aerobic conditions, J. Catal. 301 (2013) 116–124, https://doi.org/10.1016/J.JCAT.2013.01.027.

[11] R. Dhanda, M. Kidwai, Magnetically separable $CuFe_2O_4$/reduced graphene oxide nanocomposites: as a highly active catalyst for solvent free oxidative coupling of amines to imines, RSC Adv. 6 (2016) 53430–53437, https://doi.org/10.1039/C6RA08868F.

[12] X. Qiu, C. Len, R. Luque, Y. Li, Solventless oxidative coupling of amines to imines by using transition-metal-free metal-organic frameworks, ChemSusChem 7 (2014) 1684–1688, https://doi.org/10.1002/cssc.201301340.

[13] Z. Zhang, Y. Wang, M. Wang, J. Lü, L. Li, Z. Zhang, M. Li, J. Jiang, F. Wang, An investigation of the effects of CeO2 crystal planes on the aerobic oxidative synthesis of imines from alcohols and amines, Chin. J. Catal. 36 (2015) 1623–1630, https://doi.org/10.1016/S1872-2067(15)60869-5.

[14] P. Sudarsanam, A. Rangaswamy, B.M. Reddy, An efficient noble metal-free Ce-Sm/SiO_2 nano-oxide catalyst for oxidation of benzylamines under ecofriendly conditions, RSC Adv. 4 (2014) 46378–46382, https://doi.org/10.1039/c4ra04397a.

[15] S. Biswas, B. Dutta, K. Mullick, C.H. Kuo, A.S. Poyraz, S.L. Suib, Aerobic oxidation of amines to imines by cesium-promoted mesoporous manganese oxide, ACS Catal. 5 (2015) 4394–4403, https://doi.org/10.1021/acscatal.5b00325.

[16] J. Dai, J. Yang, X. Wang, L. Zhang, Y. Li, Enhanced visible-light photocatalytic activity for selective oxidation of amines into imines over TiO_2(B)/anatase mixed-phase nanowires, Appl. Surf. Sci. 349 (2015) 343–352, https://doi.org/10.1016/j.apsusc.2015.04.232.

[17] H. Huang, J. Huang, Y.-M. Liu, H.-Y. He, Y. Cao, K.-N. Fan, Graphite oxide as an efficient and durable metal-free catalyst for aerobic oxidative coupling of amines to imines, Green Chem. 14 (2012) 930, https://doi.org/10.1039/c2gc16681j.

[18] C. Su, M. Acik, K. Takai, J. Lu, S.J. Hao, Y. Zheng, P. Wu, Q. Bao, T. Enoki, Y.J. Chabal, K.P. Loh, Probing the catalytic activity of porous graphene oxide and the origin of this behaviour, Nat. Commun. 3 (2012) 1298, https://doi.org/10.1038/ncomms2315.

[19] B. Chen, L. Wang, W. Dai, S. Shang, Y. Lv, S. Gao, Metal-free and solvent-free oxidative coupling of amines to imines with mesoporous carbon from macrocyclic compounds, ACS Catal. 5 (2015) 2788–2794, https://doi.org/10.1021/acscatal.5b00244.

[20] R.D. Patil, S. Adimurthy, Copper(0)-catalyzed aerobic oxidative synthesis of imines from amines under solvent-free conditions, RSC Adv. 2 (2012) 5119–5122, https://doi.org/10.1039/c2ra20339a.

[21] R. Li, J. Byun, W. Huang, C. Ayed, L. Wang, K.A.I. Zhang, Poly-benzothiadiazoles and their derivatives as heterogeneous photocatalysts for visible light-driven chemical transformations, ACS Catal. 8 (2018) 4735–4750, https://doi.org/10.1021/acscatal.8b00407.

[22] A. Berlicka, B. König, Porphycene-mediated photooxidation of benzylamines by visible light, Photochem. Photobiol. Sci. 9 (2010) 1359–1366, https://doi.org/10.1039/c0pp00192a.

[23] B. Dutta, S. March, L. Achola, S. Sahoo, J. He, A. Shirazi Amin, Y. Wu, S. Poges, S. Pamir Alpay, S.L. Suib, Mesoporous cobalt/manganese oxide: a highly selective bifunctional catalyst for amine-imine transformations, Green Chem. 20 (2018) 3180–3185, https://doi.org/10.1039/c8gc00862k.

[24] B. Dutta, V. Sharma, N. Sassu, Y. Dang, C. Weerakkody, J. Macharai, R. Miao, A. Howell, S.L. Suib, Cross dehydrogenative coupling of N-Aryltetrahydroisoquinolines (sp³ C-H) with indoles (sp² C-H) using heterogeneous mesoporous manganese oxide catalyst, Green Chem. 19 (2017) 5350–5355, https://doi.org/10.1039/C7GC01919J.

[25] B. Dutta, S. Biswas, V. Sharma, N.O. Savage, S.P. Alpay, S.L. Suib, Mesoporous manganese oxide catalyzed aerobic oxidative coupling of anilines to aromatic azo compounds, Angew. Chemie - Int. Ed. 55 (2016) 2171–2175, https://doi.org/10.1002/anie.201508223.

[26] M.B. Gawande, R.K. Pandey, R.V. Jayaram, Role of mixed metal oxides in catalysis science—versatile applications in organic synthesis, Catal. Sci. Technol. 2 (2012) 1113, https://doi.org/10.1039/c2cy00490a.

[27] M.N. Pahalagedara, L.R. Pahalagedara, C.-H. Kuo, S. Dharmarathna, S.L. Suib, Ordered mesoporous mixed metal oxides: remarkable effect of pore size on catalytic activity, Langmuir 30 (2014) 8228–8237, https://doi.org/10.1021/la502190b.

[28] A. Elia, P.M. Aispuro, N. Quaranta, J.M. Martín-Martínez, P. Vázquez, Synthesis and characterization of new silica-titania mixed oxides obtained by sol-gel technique, Macromol. Symp. 301 (2011) 136–145, https://doi.org/10.1002/masy.201150317.

[29] H. Cui, M. Zayat, D. Levy, Sol-gel synthesis of nanoscaled spinels using propylene oxide as a gelation agent, J. Solgel Sci. Technol. 35 (2005) 175–181, https://doi.org/10.1007/s10971-005-4165-0.

[30] S. Ajaikumar, A. Pandurangan, Efficient synthesis of quinoxaline derivatives over ZrO_2/M_xO_y (M = Al, Ga, in and La) mixed metal oxides supported on MCM-41 mesoporous molecular sieves, Appl. Catal. A Gen. 357 (2009) 184–192, https://doi.org/10.1016/j.apcata.2009.01.021.

[31] W.C. Sheets, E.S. Stampler, H. Kabbour, M.I. Bertoni, L. Cario, T.O. Mason, T.J. Marks, K.R. Poeppelmeier, Facile synthesis of BiCuOS by hydrothermal methods, Inorg. Chem. 46 (2007) 10741–10748, https://doi.org/10.1021/ic7014622.

[32] B.M. Reddy, B. Chowdhury, P.G. Smirniotis, An XPS study of the dispersion of MoO_3 on TiO_2–ZrO_2, TiO_2–SiO_2, TiO_2–Al_2O_3, SiO_2–ZrO_2, and SiO_2–TiO_2–ZrO_2 mixed oxides, Appl. Catal. A Gen. 211 (2001) 19–30, https://doi.org/10.1016/S0926-860X(00)00834-6.

[33] G. Sankar, C.N.R. Rao, T. Rayment, Promotion of the metal-oxide support interaction in the Ni/TiO_2 catalyst. Crucial role of the method of preparation, the structure of TiO_2 and the $NiTiO_3$ intermediate, J. Mater. Chem. 1 (1991) 299–300, https://doi.org/10.1039/JM9910100299.

[34] D. Jiang, L. Su, L. Ma, N. Yao, X. Xu, H. Tang, X. Li, Cu-Zn-Al mixed metal oxides derived from hydroxycarbonate precursors for H_2S removal at low temperature, Appl. Surf. Sci. 256 (2010) 3216–3223, https://doi.org/10.1016/j.apsusc.2009.12.008.

[35] B.M. Reddy, I. Ganesh, Characterization of La_2O_3-TiO_2 and V_2O_5/La_2O_3-TiO_2 catalysts and their activity for synthesis of 2,6-dimethylphenol, J. Mol. Catal. A Chem. 169 (2001) 207–223, https://doi.org/10.1016/S1381-1169(00)00564-1.

[36] A.S. Kulkarni, R.V. Jayaram, Liquid phase catalytic transfer hydrogenation of aromatic nitro compounds on $La_{1-x}Sr_xFeO_3$ perovskites prepared by microwave irradiation, J. Mol. Catal. A Chem. 223 (2004) 107–110, https://doi.org/10.1016/j.molcata.2003.12.042.

[37] V.V. Zyryanov, Mechanochemical synthesis and thermal behavior of metastable mixed oxides in the CaO-Sb_2O_3-Bi_2O_3 system, Inorg. Mater. (Transl. Neorg. Mater.) 39 (2003) 1163–1171, https://doi.org/10.1023/A:1027301626107.

[38] V.V. Zyryanov, V.I. Smirnov, M.I. Ivanovskaya, Mechanochemical synthesis of crystalline compounds in the Bi_2O_3 – GeO_2 system, Inorg. Mater. Appl. Res. 41 (2005) 618–626, https://doi.org/10.1134/S0036023615050083.

[39] J. Wei, Z. Sun, W. Luo, Y. Li, A.A. Elzatahry, A.M. Al-Enizi, Y. Deng, D. Zhao, New insight into the synthesis of large-pore ordered mesoporous materials, J. Am. Chem. Soc. 139 (2017) 1706–1713, https://doi.org/10.1021/jacs.6b11411.

[40] A.S. Poyraz, C.-H. Kuo, S. Biswas, C.K. King'ondu, S.L. Suib, A general approach to crystalline and monomodal pore size mesoporous materials, Nat. Commun. 4 (2013) 2952, https://doi.org/10.1038/ncomms3952.

[41] N.D. Wasalathanthri, A.S. Poyraz, S. Biswas, Y. Meng, C.H. Kuo, D.A. Kriz, S.L. Suib, High-performance catalytic CH_4 oxidation at low temperatures: inverse micelle synthesis of amorphous mesoporous manganese oxides and mild transformation to $K_{2-x}Mn_8O_{16}$ and μ-MnO_2, J. Phys. Chem. C. 119 (2015) 1473–1482, https://doi.org/10.1021/jp5108558.

[42] A.S. Poyraz, W. Song, D. Kriz, C.H. Kuo, M.S. Seraji, S.L. Suib, Crystalline mesoporous $K_{2-x}Mn_8O_{16}$ and ε-MnO_2 by mild transformations of amorphous mesoporous manganese oxides and their enhanced redox properties, ACS Appl. Mater. Interfaces 6 (2014) 10986–10991, https://doi.org/10.1021/am502846e.

[43] W. Song, A.S. Poyraz, Y. Meng, Z. Ren, S.Y. Chen, S.L. Suib, Mesoporous Co_3O_4 with controlled porosity: inverse micelle synthesis and high-performance catalytic CO oxidation at -60 °C, Chem. Mater. 26 (2014) 4629–4639, https://doi.org/10.1021/cm502106v.

[44] Z. Luo, A.S. Poyraz, C.H. Kuo, R. Miao, Y. Meng, S.Y. Chen, T. Jiang, C. Wenos, S.L. Suib, Crystalline mixed phase (anatase/rutile) mesoporous titanium dioxides for visible light photocatalytic activity, Chem. Mater. 27 (2015) 6–17, https://doi.org/10.1021/cm5035112.

[45] R. Miao, Z. Luo, W. Zhong, S.-Y. Chen, T. Jiang, B. Dutta, Y. Nasr, Y. Zhang, S.L. Suib, Mesoporous TiO_2 modified with carbon quantum dots as a high-

performance visible light photocatalyst, Appl. Catal. B Environ. 189 (2016) 26–38, https://doi.org/10.1016/J.APCATB.2016.01.070.

[46] T. Jiang, S. Du, T. Jafari, W. Zhong, Y. Sun, W. Song, Z. Luo, W.A. Hines, S.L. Suib, Synthesis of mesoporous γ-Fe₂O₃ supported palladium nanoparticles and investigation of their roles as magnetically recyclable catalysts for nitrobenzene hydrogenation, Appl. Catal. A Gen. 502 (2015) 105–113, https://doi.org/10.1016/J.APCATA.2015.05.013.

[47] T. Jiang, A.S. Poyraz, A. Iyer, Y. Zhang, Z. Luo, W. Zhong, R. Miao, A.M. El-Sawy, C.J. Guild, Y. Sun, D.A. Kriz, S.L. Suib, Synthesis of mesoporous iron oxides by an inverse micelle method and their application in the degradation of orange II under visible light at neutral pH, J. Phys. Chem. C. 119 (2015) 10454–10468, https://doi.org/10.1021/acs.jpcc.5b02057.

[48] T. Jiang, W. Zhong, T. Jafari, S. Du, J. He, Y.J. Fu, P. Singh, S.L. Suib, Siloxane D4 adsorption by mesoporous aluminosilicates, Chem. Eng. J. 289 (2016) 356–364, https://doi.org/10.1016/j.cej.2015.12.094.

[49] O.O.E. US EPA, Basics of Green Chemistry, EPA.GOV, (2013) (Accessed 12, August 2018), https://www.epa.gov/greenchemistry/basics-green-chemistry.

[50] Y. Nosaka, A.Y. Nosaka, Generation and detection of reactive oxygen species in photocatalysis, Chem. Rev. 117 (2017) 11302–11336, https://doi.org/10.1021/acs.chemrev.7b00161.

[51] D.A. Kriz, J. He, M. Pahalagedara, S.L. Suib, Response to Comments on the application of the Scherrer equation in "Copper aluminum mixed oxide (CuAl MO) catalyst: a green approach for the one-pot synthesis of imines under solvent-free conditions", by Suib et al. [Appl. Catal. B: environ, 188 [2016] 2, Appl. Catal. B Environ. 202 (2017) 704–705, https://doi.org/10.1016/J.APCATB.2016.09.049.

[52] C.-Y. Hu, K. Shih, J.O. Leckie, Formation of copper aluminate spinel and cuprous aluminate delafossite to thermally stabilize simulated copper-laden sludge, J. Hazard. Mater. 181 (2010) 399–404, https://doi.org/10.1016/J.JHAZMAT.2010.05.024.

[53] Http:/xpssimplified.com/elements/copper.php, XPS Interpretation of Copper, (2015), pp. 3–6 (Accessed 05, May 2018), https://xpssimplified.com/elements/copper.php.

[54] NIST XPS Database, (n.d.). https://srdata.nist.gov/xps/elm_Spectra_query.aspx?Elm1 = Al&LD1 = 2p&Elm2 = &LD2 = &Elm3 = &LD3 = &Elm4 = &sType = PE (Accessed 05, May 2018).

[55] X. Huang, M. Zheng, Y.X. Wang, D.D. Li, Y.J. Zhao, Selective reduction of Chloronitrobenzene to Chloroaniline on Ni/Al₂O₃ catalysts got-up ionic liquids, Adv. Mater. Res. 233 (2011) 2904–2908 doi:10.4028/www.scientific.net/AMR.233-235.2904.

[56] B. Karimi, A. Biglari, J.H. Clark, V. Budarin, Green, transition-metal-free aerobic oxidation of alcohols using a highly durable supported organocatalyst, Angew. Chemie - Int. Ed. 46 (2007) 7210–7213, https://doi.org/10.1002/anie.200701918.

[57] S. Biswas, K. Mullick, S.Y. Chen, D.A. Kriz, M. Shakil, C.H. Kuo, A.M. Angeles-Boza, A.R. Rossi, S.L. Suib, Mesoporous Copper/Manganese oxide catalyzed coupling of alkynes: evidence for synergistic cooperative catalysis, ACS Catal. 6 (2016) 5069–5080, https://doi.org/10.1021/acscatal.6b00717.

[58] K.N. Tayade, M. Mishra, Catalytic activity of MCM-41 and Al grafted MCM-41 for oxidative self and cross coupling of amines, J. Mol. Catal. A Chem. 382 (2014) 114–125, https://doi.org/10.1016/j.molcata.2013.11.001.

[59] J.M. Pérez, R. Cano, M. Yus, D.J. Ramõn, Straightforward synthesis of aromatic imines from alcohols and amines or nitroarenes using an impregnated copper catalyst, European J. Org. Chem. 2012 (2012) 4548–4554, https://doi.org/10.1002/ejoc.201200319.

[60] X.J. Yang, B. Chen, X.B. Li, L.Q. Zheng, L.Z. Wu, C.H. Tung, Photocatalytic organic transformation by layered double hydroxides: highly efficient and selective oxidation of primary aromatic amines to their imines under ambient aerobic conditions, Chem. Commun. 50 (2014) 6664–6667, https://doi.org/10.1039/c4cc01671h.

[61] S. Furukawa, Y. Ohno, T. Shishido, K. Teramura, T. Tanaka, Selective amine oxidation using Nb₂O₅ photocatalyst and O₂, ACS Catal. 1 (2011) 1150–1153, https://doi.org/10.1021/cs200318n.

[62] D.B. Ushakov, M.B. Plutschack, K. Gilmore, P.H. Seeberger, Amine oxidation factors influencing the regioselectivity of the oxidation of asymmetric secondary amines with singlet oxygen, Chem. A Eur. J. 21 (2015) 6528–6534, https://doi.org/10.1002/chem.201500121.

[63] C.F. Grellet Bournonville, J.C. Díaz-Ricci, Quantitative determination of superoxide in plant leaves using a modified NBT staining method, Phytochem. Anal. 22 (2011) 268–271, https://doi.org/10.1002/pca.1275.

[64] D.R. Kearns, Physical and chemical properties of singlet molecular oxygen, Chem.Rev. 71 (1971) 395–427, https://doi.org/10.1021/cr60272a004.

[65] R. Poupko, I. Rosenthal, Electron transfer interactions between superoxide ion and organic compounds, J. Phys. Chem. 77 (1973) 1722–1724 (Accessed 23, July 2018), https://pubs.acs.org/sharingguidelines.

[66] E.A. Mayeda, A.J. Bard, Experimental section, J. Am. Chem. Soc. J. 95 (1973) 6223–6226, https://doi.org/10.1021/ja00800a012 (Accessed 23, July 2018).

[67] B. Chen, J. Li, W. Dai, L. Wang, S. Gao, Direct imine formation by oxidative coupling of alcohols and amines using supported manganese oxides under an air atmosphere, Green Chem. 16 (2014) 3328–3334, https://doi.org/10.1039/c4gc00336e.